Article

Intrinsic Environmental Vulnerability as Shallow Landslide Susceptibility in Environmental Impact Assessment

Laura Turconi [1,*], **Fabio Luino** [1], **Mattia Gussoni** [2], **Francesco Faccini** [1,3], **Marco Giardino** [4] **and Marco Casazza** [5,*]

[1] Istituto di Ricerca per la Protezione Idrogeologica, Consiglio Nazionale delle Ricerche, Strada della Cacce 73, 10135 Torino, Italy; fabio.luino@irpi.cnr.it (F.L.); faccini@unige.it (F.F.)
[2] Freelance geographer, Via Leonardo da Vinci 45, 20062 Cassano d'Adda (Milano), Italy; mattia.gussoni86@gmail.com
[3] Department of Earth, Environment and Life Sciences, University of Genoa, Corso Europa 26, 16132 Genova, Italy
[4] Department of Earth Sciences, University of Turin, Via Valperga Caluso 35, 10125 Torino, Italy; marco.giardino@unito.it
[5] Department of Engineering, Parthenope University of Napoli, Centro Direzionale, Isola C4, 80143 Napoli, Italy
[*] Correspondence: laura.turconi@irpi.cnr.it (L.T.); marco.casazza@uniparthenope.it (M.C.)

check for updates

Abstract: This work investigated the susceptibility factors that trigger shallow landslides. In particular, the objective of the research was the implementation of a method to determine the relevant factors that can trigger shallow landslide events. However, with respect to the existing methods, the integration with historical datasets and the inclusion of spatial factors displaying dynamics in the same characteristic timescales were specific features of the developed tool. The study area included the watersheds of the Sessera and Strona rivers in the alpine area of the Province of Biella (Piedmont, NW Italy). The method was developed and tested from two sub-datasets derived from an integrated dataset that referred to an intense event, involving the same area, that occurred in 1968 (2–3 November). This allowed the implementation of an integrated representation of landslides' predisposing factors and the identification and classification in different groups of the areas susceptible to geo-hydrological instability processes. The previously existing databases were verified and integrated into a geographic information system (GIS) environment, giving a potentially sharable source of information for planning purposes. The obtained maps represent a metric of one of the possible intrinsic environmental vulnerability factors for the area under study. Consequently, this method can represent a future instrument for determining the intrinsic environmental vulnerability dependent on landslides within an environmental impact assessment (EIA), as required by the most recent European regulation on EIA. Moreover, the shared information can be used to implement informed policy and planning processes, based on a bottom-up approach. In particular, the availability online of landslide susceptibility maps could support the generation of augmented information—useful for both local administrators and planners as well as for stakeholders willing to implement specific projects or infrastructure in vulnerable areas, such as mountains.

Keywords: landslide susceptibility; GIS; environmental vulnerability; environmental impact assessment; mountain

1. Introduction

The huge population growth, the expansion of economic activities, and the increase of intensive land exploitation and infrastructures are some of the potential obstacles to mountains' sustainable development [1]. These obstacles, in turn, require further attention, considering that these areas are prone to several types of natural hazards. It is especially important to develop sustainable and resilient approaches in relation to the communities that are at risk [2]. Consequently, knowledge of the intrinsic environmental vulnerability, also known as environmental sensitivity, of mountain areas is especially relevant in implementing any project, as indicated by the latest European directive on environmental impact assessment [3].

Within any environmental impact assessment, a sensitivity analysis should enable the identification of intrinsic risks and the potential impacts of projects on the sustainability and resilience of the considered area [4]. Prior to considering the anthropogenic pressures generated by any project, the intrinsic vulnerability should be evaluated. In the case of mountain areas, landslides are the seventh largest killer among natural disasters [5], contributing to about 17% of global mortality [6]. The generated economic losses and casualties are greater than generally recognized. For example, in the United States, landslides have caused an economic loss estimated between 1 and 3.6 billion US dollars (converted to 2010 dollars) [7]. Similarly, Japanese annual losses have been reported to be between 4 and 6 billion US dollars [8]. Moreover, the most disastrous landslides have claimed as many as 100,000 lives [9]. On the other hand, the alteration of the natural environment and ecosystem services can be equally relevant [10].

The dynamics of factors contributing to the environmental vulnerability of an area have different characteristic timescales. Some of them relate to the local evolution of anthropogenic activities. Consequently, the impacts affecting the vulnerability might be evident within a shorter timescale. This is the case, for example, of the introduction of engineered modification of watercourses. In the case of weather pattern modifications, depending on climate change, they might appear within a centennial timescale. Being identified among the most relevant factors in triggering landslides [11], the modification of rainfall patterns may increase the landslide frequency and/or intensity. It is well known, in fact, that warmer air temperature is linked to an increase in atmospheric water vapor content, which, in turn, may increase the potential for more frequent and intense precipitation events [12]. On longer timescales, paleo proxies indicate that temperatures and CO_2 concentrations co-varied in the past on timescales ranging from the glacial cycles, during the Quaternary, to the more recent Little Ice Age (LIA) and the inter-annual El Niño–Southern Oscillation (ENSO) variability. Using an ensemble of experiments with an Earth system model of intermediate complexity, a pronounced timescale dependence between CO_2 and temperature variations was found, with a maximum on centennial scales. Furthermore, up to centennial scales, the land carbon response to climate dominates the CO_2 signal in the atmosphere, while on longer timescales the ocean becomes important and eventually dominates on multi-millennial scales [13].

Obviously, natural factors also have their characteristic timescales. With respect to climate, Sun–Earth interplay and other planetary relations should be considered [14–16]. Concerning the lithosphere, each soil body is formed by a combination of some specific pedogenic processes (SPP). The whole set of SPP may be grouped in accordance with their essence, characteristic times (rates), and reversibility/irreversibility [17]. In terms of characteristic times (rates), they may be arranged in three main groups—rapid (10^{1-2} years), medium-rate (10^{3-4} years), and slow (10^{5-6} years). Thus, anthropogenic activities and climate change have the same timescales of rapid SPP.

In modeling the natural vulnerability of a mountain area in relation to its susceptibility to shallow landslides, the selection of factors with longer characteristic timescales would allow the disentanglement of natural landscape dynamics from human-induced pressures. Moreover, the number of factors included in landslide susceptibility models could be reduced. In fact, anthropogenic forcing might alter the long-term validity and applicability of such models for forecast purposes. On the other hand, temporal scales are also relevant in the determination of impacts in environmental impact

assessment practices [18]. Since the factors with longer timescales better define the nature of the intrinsic environmental sensitivity of an area, they should be preferred in a first assessment of the baseline conditions.

Limited to intrinsic factors with longer characteristic timescales, thus excluding the effects of weather conditions on the evolution of slope instability processes, this study defined a GIS-based tool to evaluate the environmental spatial sensitivity to shallow landslides. This was done in terms of spatial susceptibility, using an area prone to the development of shallow landslides, as test for the proposed tool. This work implemented an existing method [19], in order to assess the intrinsic environmental vulnerability of a mountain area, where an environmental impact assessment might be required. Section 2 of this paper describes the applied method and introduces the case study. Section 3 focuses on applying and testing the model with the selected case study. Section 4 discusses the results, and in Section 5, the conclusions and future research perspectives are defined.

2. Methodology

2.1. Reference Method

The present method was based on a previous approach [19], which is currently the most widely applied due to its performance and possibility of being converted into appropriate spatial maps of landslide susceptibility [20–22].

For this method, a set of factors considered to be the triggers of the observed instability are first selected (e.g., [23]). Then, their interplay is considered in assessing the landslide susceptibility in a given area [24]. In particular, for each analyzed factor viewed as a landslide trigger, a set of variability classes is defined, in order to evaluate their relative impact on the overall instability phenomenon. The relative impact factor (IF) is weighted against the abundancy of landslides within each class.

Considering the existence of j different classes, each of them has a relative IF, indicated as $IF_{rel,j}$. The weight for the j-th class is indicated with w_j. Then, the total impact factor, related to landslide susceptibility, indicated as IF_{tot}, is defined as

$$IF_{tot} = \sum_{j=1}^{k} IF_{rel,j} \times w_j \qquad (1)$$

being

$$IF_{rel,j} = \frac{IF_i}{IF_{i(max)}} \times 100 \qquad (2)$$

and

$$IF_i = \frac{a_i}{b_i} = \frac{N(f_i)/N(F)}{N(s_i)/N(S)}; \ w_j = \frac{IF_{min,j}}{\sum_{j=1}^{k} IF_{min,j}}; \ j = 1, \ldots, k. \qquad (3)$$

2.2. Definition of the Case Study

The study area, about 150 km^2 wide, extends from the southern border of the Pennine Alps (NW Italy) to the hills (granitic massif of Biella). The study area is delimited by the drainage basins of the Strona and Sessera rivers, both located in the northern part of the Piemonte region (NW Italy). The Po Valley and the Pennine Alps, in the sub-sector of Biellesi and the Cusiane Alps [25], constitute a further geographical limitation of this area. Such an area exhibits a characteristic central relief, known as the Rubello–Prapiano–Massaro massif, which forms a natural barrier between the alpine and flatland zones. The massif, ranging from west to east between 1400 m and 1200–1300 m, respectively, stretches in parallel along two main fault lines, the Cremosina and the Insubric lines. The latter separates the Pennine Alps (NW) from the Meridional Alps (SE). Figure 1 shows a map of the main geographical and geological features of the study area.
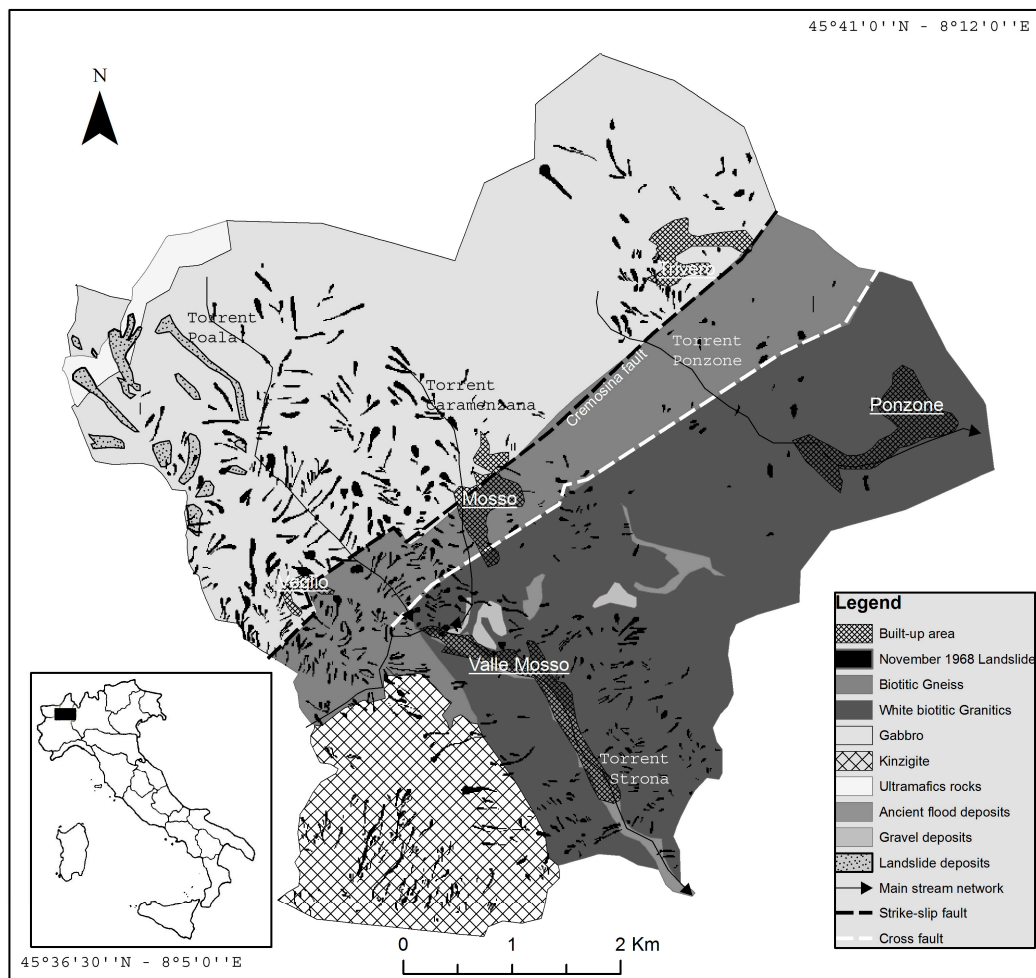
Figure 1. Map of the main geographical and geological features of the study area in the Piemonte region (NW Italy).

The bedrock is prevailingly made of leucocratic gabbro and coarse-grained pyroxene–amphibole gabbro, having a locally parallel texture together with lenses of finely grained ultramafic rocks, often converted to diaftorites, being dark green to blackish-colored. Besides the characteristic granite, biotite-rich diorite also occurs with minor amounts of encrusted muscovite.

An irregularly thick weathered layer covers the granite, into which the middle sector of the Strona river basin is incised, that is densely covered with woodland. Both pedogenic and vegetation products are the basic components for detrital production. In fact, they are found in the main constituents of mass movements, generated over fully saturated slopes in the case of prolonged and intense rainfall.

Previous on-site monitoring activities gave an insight into how, apart from the mother-rock characteristics, the soil cover depth in this area is influenced by the landscape slope and morphology. In particular, in the case of a deeper soil thickness in correspondence to less-inclined slopes, these areas were shown to be subjected less to the erosive power of the running waters as well as to gravity-driven soil losses. Moreover, the soil cover depth decreases with increased elevations and more marked reliefs, where outcrops are more likely to occur.

2.3. Analyzed Susceptibility Factors

The historical analysis of instability processes in the study area [26] evidenced that soil slips and debris flows were the most frequent [27,28]. Considering the existing literature [29], the most meaningful triggering factors that should be included in the vulnerability assessment are lithology; morphology, concavity, and convexity of slopes; slope dipping; slope aspect; distance from water bodies;

and land use. These factors were selected, depending on the availability of useful databases for their characterization. In particular, the morphological and lithological characteristics, the conformation of the drainage network, and the land use of the area under study served as a basis for this research. In order to define landslide susceptibility as a function of these parameters, an inventory of historical landslides was realized. In parallel, the data, necessary for characterizing the predisposing factors, were searched for and found. Original data were processed through geographical information system (GIS) software, as previously done in another work [30], to create a set of thematic maps, with each map corresponding to a single instability factor to be analyzed. Table 1 shows the list of databases used as a basis for the analysis of instability predisposing factors. The list of derived GIS thematic maps is also given.

Table 1. Database sources and GIS map derived for the assessment of susceptibility.

Source	Original Data Format	Obtained Information/Map
Digital Elevation Model (cell size 10 m)	Raster File	Aspect (File.Raster) Slope (File.Raster) Contour's Curvatures (File.Raster)
Geological maps (scale 1:5000 and 1:10,000)	.PDF File Paper	Lithologic map (File.Shape) Lithologic map (File.Raster)
Aerial photos of the flood event 1968	Black and White Photos	Land use map (File.Shape) Land use map (File.Raster) Map of the stream network processes due to the 1968 flood (File.Shape)
Drainage network (scale 1:10,000)	Shape File	Map of the distances from stream incisions (File.Raster)

The obtained thematic maps were re-classified through a comparison with a selected sub-set of landslide data, centered on the same area, in order to maximize the correspondence (LSI$_{corr}$) between the landslide density for a single class and the value of the corresponding landslide susceptibility index (IF$_{rel,j}$). In particular, a test dataset, i.e., a group of data used for evaluating the susceptibility inside the area of study, was extracted out of the landslide historical inventory. Another sub-set, belonging to the same inventory, was considered as a verification dataset called the test set. This test set was used, after the parameterization of susceptibility, to verify, re-calibrate, and validate the estimation method in use. Finally, a landslide susceptibility map was generated, covering a 25 km^2 area, centered on the upper Strona river basin and a part of the Ponzone river, a tributary of the Sessera Valley in the opposite slope (see Figure 1).

Furthermore, the study was divided into the following phases: construction of the landslide inventory, data search for the characterization of the predisposing factors, construction of thematic maps suitable for the characterization of predisposing factors, and intersection of information layers, summary of results, and graphic restitution.

During the first step, historical data were collected to re-construct the past landslide events. Historical analysis is a key tool when studying the problems connected to slope instability and stream flood processes. In fact, it allows (a) the detection of areas that, due to geo-morphological and geo-structural conditions, land use, and climatic regime, appear as the most sensitive to the triggering of processes, thus allowing the possible factors leading to instability to be detected, (b) the identification of the laws, by which the susceptibility factors exert their control in triggering the conditions of the instability processes, through a back-analysis procedure, and (c) the projection into the future of the acquired historical information and, by this way, the possible risk scenarios arising from man-made land modifications can be identified. This occurs according to the principle that the instability processes are liable to occur in areas historically affected by similar processes [26,31–35].

The reconstruction of the effects induced by historical floods and gravitational processes implied four steps: (1) search of data sources, (2) acquisition of the information and cartographic and/or photographic documents, (3) data selection, analysis, and validation, and (4) GIS transposition of the data.

The data collection was based on the examination of historical sources (e.g., newspaper chronicles, bibliographies, technical manuscripts, and all kinds of inherent documents) preserved in the archives of the Italian National Research Council – Institute for Research on Hydrogeologic Risks (CNR-IRPI) as well as in the archives of some municipalities belonging to the area under study.

The available data were represented in a GIS environment (using the Technical Regional Map, at 1:10,000 scale, as the base map) to draw a geo-referenced database, which was useful for further spatial analyses. Every single identified process was represented either as a punctual or a polygonal element, depending on the detail of the available knowledge. The database records, combined to each geometrical feature, were composed by a group of attributes, which define the typology, geographical location, and triggering period of the process.

The historical analysis allowed the listing of 148 relevant rainfall events, since 1825, which involved 15 municipalities in the eastern part of Biella Province, Piemonte region, NW Italy (Table 2). Single events may have caused the triggering of more than one related process. This is why the number of recorded rainfall events and the number of instability processes does not coincide.

Table 2. Main rainfall events and related geo-hydrological processes in the area of study. Municipalities abbreviations: CO—Coggiola, P—Pray, and VM—Valle Mosso.

Event Date (year, month, day)	Main Stream	Municipality	Geo-hydrological Processes
1854, July 2	Strona	VM	Landslide
1857, October 21–22	Strona	VM	Flood
1878, August 3	Sessera, Strona	CO, VM	Flood
1879, May 29	Strona	VM	Flood, Landslide
1907, October	Strona	VM	Landslide
1908, May 26	Sessera, Strona	CO, VM	Flood, Landslide
1922, September 5	Sessera	CO	Landslide
1924, October 7–10	Sessera	CO	Flood, Landslide
1926, May 26	Sessera	CO	Flood, Landslide
1927, June 28	Sessera, Strona	CO, VM	Flood, Landslide
1928, April 1	Sessera	P	Landslide
1930, July 24	Sessera	P	Flood
1937, November 2	Sessera	P	Landslide
1938, June 14	Sessera	CO	Landslide
1948, September 7	Strona	VM	Flood, Landslide
1951, November 10–11	Sessera, Strona	CO, VM	Flood, Landslide
1953, September/October	Sessera	P	Flood
1956, November 28	Sessera	CO	Flood
1959, May 3	Strona	VM	Landslide
1966, October 11	Strona	VM	Landslide
1967, June 10	Sessera	P	Flood, Landslide
1967, September 14	Sessera	P	Flood, Landslide
1968, June	Sessera	CO	Flood, Landslide
1968, November 2–3	Sessera, Strona	CO, P, VM	Flood, Landslide
1976, November 26	Sessera	CO, P	Landslide
1977, May 1–3	Sessera, Strona	CO, P, VM	Flood, Landslide
1977, June 18	Sessera	CO	Landslide
1977, July 28–31	Sessera	P	Flood
1977, October 10	Sessera	CO, P	Flood, Landslide
1979, October 14–15	Sessera, Strona	CO, P, VM	Flood, Landslide
1981, September 22–23	Sessera	CO, P	Flood, Landslide
1985, May 16	Strona	VM	Landslide

Table 2. *Cont.*

Event Date (year, month, day)	Main Stream	Municipality	Geo-hydrological Processes
1985, June 3–4	Sessera	CO	Flood, Landslide
1987, August 23–25	Sessera	P	Landslide
1988, July 1	Sessera	P	Landslide
1993 May 20	Sessera	P	Landslide
1994, May 18	Sessera	CO	Landslide
1994, November 5	Sessera, Strona	CO, VM	Landslide
1998, July 1	Sessera	P	Landslide
2000, October 13–17	Sessera	P	Landslide
2002, May 2–3	Sessera	P	Landslide
2002, June 6	Sessera	P	Flood, Landslide

The recorded historical events showed a greater susceptibility to geo-hydrological effects (mainly landslides and floods) in the spring/early summer (mainly in May) and autumn (mainly in October and November), corresponding to the year's rainiest periods for this area.

2.4. The Test Event

During the first days of November 1968, a heavy rainfall event was recorded in the area under study. In some sectors, it exhibited exceptional characteristics, which caused the flooding of countryside and several inhabited areas. The consequences were catastrophic, especially in the valleys upstream of the Biella municipality (Strona, Sessera, and Cervo rivers), a rich industrial area in NW Italy for the many textile companies.

The exceptionality and persistence of rainfall in some areas was such that in many localities the historical highs recorded in the thirty years between 1921 and 1950 were exceeded. The average rainfall amounts in the considered basins during the event were double or triple that of the corresponding historical average rainfall for the same month (i.e., November). In particular, on November 2, peaks, with an intensity of 60 mm/h, were recorded in the afternoon. The isohyets map that refers to November 2, 1968 (from 16:00 to 22:00) is representative of the extraordinary nature of this pluviometric event [36]. Daily peaks of 220 mm were also recorded in the upper basin of the Strona and the Sessera streams, as visible from the pluviograms, which recorded significant rainfall intensities for the study area (Figure 2).
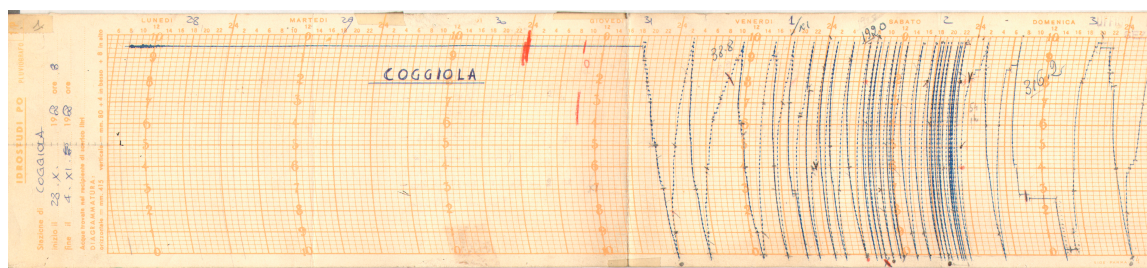
Figure 2. Original rainfall track recorded at Coggiola meteorological station. The maximum peak was recorded around 9 pm, with a rainfall amount 30 mm recorded in 30 min. The pluviogram has a rainfall amount resolution of 0.2 mm. The interval, from the bottom to the top of the pluviogram covers a span of 10 mm. The time resolution, reported on the horizontal axis, has a resolution of 1 h.

The most intense phase of the rain began at 17:00, within the area centered in the villages of Pettinengo and Camandona. A limited area of about 50 km^2 was hit by intense precipitation during just 4 h. Past analyses of both pluviograms and rainfall distribution graphs displayed two distinct phases. The first, between 18:00 and 19:30, with precipitation peaks of 29 mm/30 min (Coggiola municipality, time slot from 18:00 to 18:30). The second stage of the event occurred between 20:00 and 21:00. During the last phase, the weather stations in the municipalities of Camandona, Pettinengo, and Trivero recorded precipitation intensities in the order of 60 mm/h.

As a consequence, a very high number of landslides occurred, mainly centered in the municipality of Trivero (eastern side of Biella Province, Piemonte region, NW Italy). Several erosion processes along the hydrographic network and extensively flooded areas gave the alluvial event a catastrophic dimension (Figure 3).

| (a) | (b) |

Figure 3. Some effects of the 1968 flood event are visible along the drainage network (**a**) and the slope (**b**).

In the Strona Valley alone, 58 victims were recorded, while in the whole of the Piemonte region, more than 70 victims were recorded. The losses detected in this area reached exceptional levels. In fact, in some municipalities the production assets were 90% destroyed. Overall, in the Province of Vercelli, there were 376 affected buildings, of which 277 were in the Biella area alone, while around 13,000 people were left without work. Substantial damage was also suffered by the homes and the connection infrastructures (bridges, roads), so that for several hours many municipalities were isolated.

The distribution map of the landslides gave a global view of the numerous landslides that occurred in the Strona Valley during these days. By dividing the surface area of the Strona river catchment area into regular meshes of 1 km^2, the maximum peak of 91 landslides/km^2 was reached (municipality of Valle Mosso). The most common forms of observed soil degradation processes were [37]:

- Landslides developed along pre-existing discontinuity surfaces, mostly between the crystal-lined rock substrate and the eluvio-colluvial layer. This type of instability is usually observed on granitic sandy coulters. Landslides of this type have a prevalence of flattened solids, with a smooth sliding surface, represented by a variable inclination plane;
- Landslides developed along sliding planes of neo formation. In this case, the failures are promoted by the progressive imbibition of the ground and other factors that lead to overcoming the resistance to the cutting. The phenomenon is typical of pasture or grassland, being favored by local slope variations, building works, or excavations. The movement occurs by the rotation and integral translation of the plate;
- Gully erosion due to the flow of surface runoff water either on the bottom of usually dry valleys or on their sides;
- Rapid earth flow.

2.5. Analysis of Instability Factors

The landslide hazard of an area, defined as the probability of a landslide event of a given intensity, is expressed by a given interval [38]. The mapped results describe the distribution of spatial (geographical) landslide occurrence probability. Often, the temporal probabilistic factor is difficult to determine. This is why past studies have expressed the concept of susceptibility for the predisposition to landslides, described either in qualitative or quantitative terms, in a study area [23,39]. This method is based on two main assumptions: (a) the knowledge and mapping of historical events should be

integrated in the study of an area and (b) slope phenomena are likely to occur in the future in areas previously affected by analogous events and be characterized by a set of similar parameters (e.g., topographical, lithological, and land use).

The method used for the determination of susceptibility is based on the identification and spatial characterization of a set of control factors, on the quantification of the spatial relations between those factors, and an archive of previous landslides [23]. This method assumes that future landslides will take place under the same conditions as those of the past. Moreover, it represents an application of Bayes theorem, according to which frequency of each map unit is similar to the landslide occurrence probability. Each instability frequency or density represents the probability of the occurrence of a future event.

First, a set of instability predisposing factors was defined (e.g., lithology, land use, and slopes). This set was divided into classes. Then, a relative index was calculated through overlapping the landslides map with each single-factor map. The flowchart related to the calculation process is represented in Figure 4.
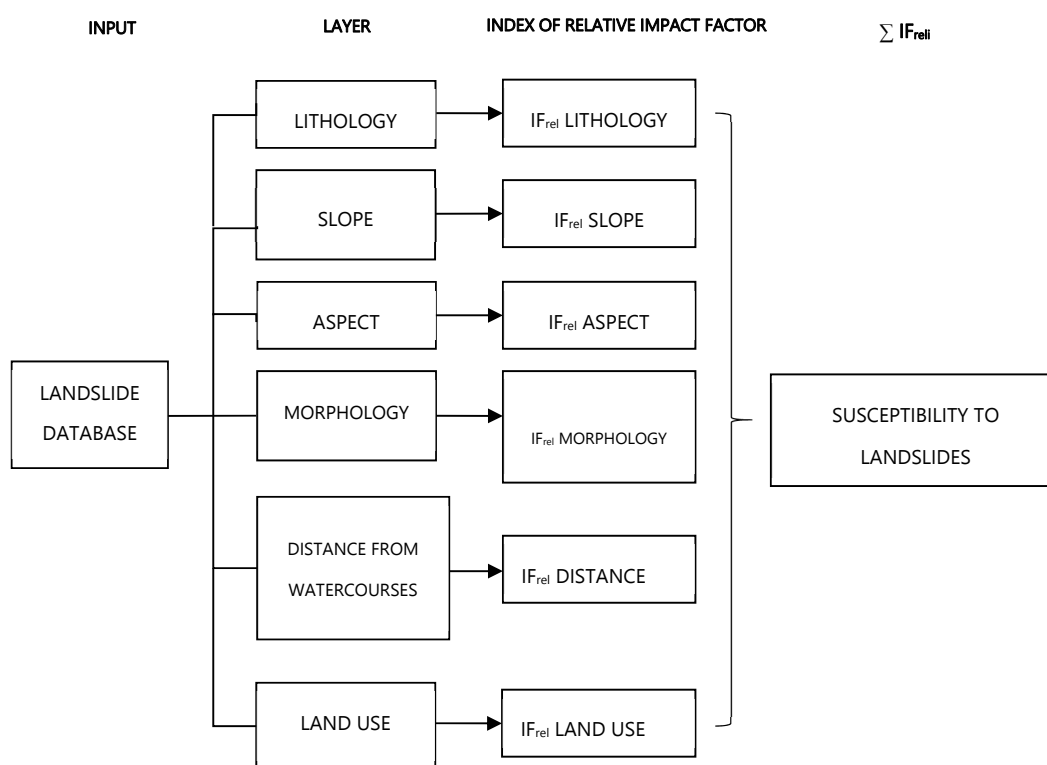

Figure 4. Flowchart of analysis for evaluation of the final impact factor (IF_{rel}).

2.5.1. Lithology

Lithology is one of the most important factors in the control of slope stability. In fact, the type of bedrock substantially affects the mechanical properties of the materials forming the slopes, e.g., permeability and shear stress.

The basic lithological information was drawn from the technical cartography of the municipalities included in the area under study (map scales: 1:10,000 and 1: 5000). The content of such cartographic documents was checked on-site. The gathered information was geo-referenced, digitized in vectorial format, and converted into raster format by adopting 10×10 m cells, corresponding to the detail of the base maps.

The acquired data showed that, out of the 8 lithological classes identified in the territory under study, the lithological units most widely determined around the landslide-prone sites were the gabbro, leucogranite (white granite), biotitic gneiss, and kinzigite rocks (Figure 5).
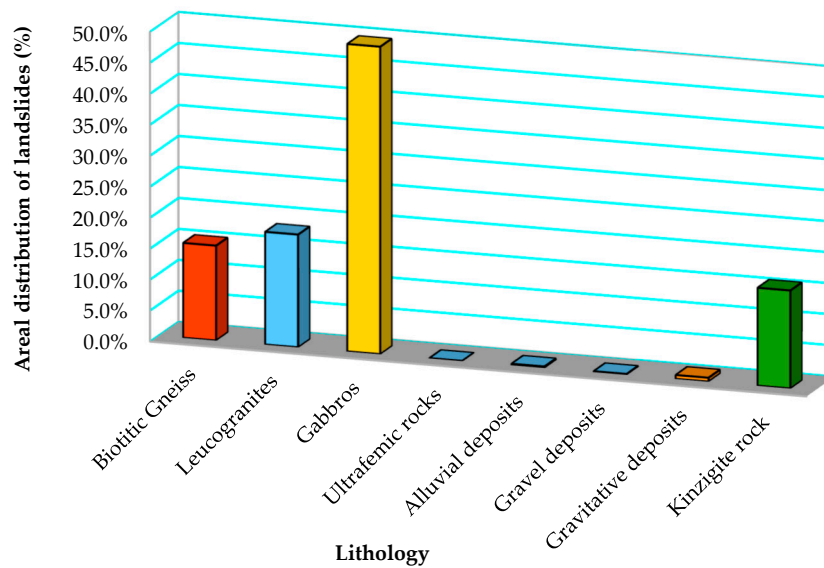
Figure 5. Areal distribution of landslides (%) in relation to the lithological substrate or bedrock (lithology).

2.5.2. Morphology: Concavity and Convexity Slope

The slope curvature with respect to the maximum dipping (angle) is significant for stability and influences the overland flow and drainage of running waters. In particular, shallow landslides seem to occur preferably in topographical convergence zones, where favorable conditions occur for stagnation, an increase of pore pressure, and reduction of shear stress for loose materials [40]. In particular, the drainage in a concave slope leads to an increase in the water pressure within pores and an accumulation in the surface formations. This favors the occurrence of surface movements.

The morphology (distribution of the convex–concave shaped slope surfaces) of the study area was re-constructed through the GIS-based elaboration of the digital elevation model (DEM). The available DEM refers to the present-day slope conditions, even if not representative of the situation prior to the 1968 flood, and allows the determination of the rapidly evolving processes that control the slope morphology (trigger conditions for landsliding, masking or erasing the depositional forms by natural or anthropic agents). A morphology map was obtained, which also identified the watersheds and valley areas. All the watersheds, which can have important ground effects during intense rainfall events, were identified.

2.5.3. Slope

The dipping angle plays an important role for slopes. In fact, it is the control factor determining the velocity and impact energy of the sliding masses. The dip value defines, for a given exposed material along the slope, the 'distance' from the natural equilibrium conditions, expressed through the internal friction angle.

The dip-slope map was drawn from a GIS-based DEM elaboration. In the map, 6 slope angle intervals were defined as <15°, 15–20°, 20–25°, 25–30°, 30–35°, and >35°. In order to assess the areal landslide density inside each class and for calculating the relevant landslide susceptibility index, a slope angle was assigned corresponding to the position of the detachment niche for every landslide reported in the instability map.

2.5.4. Aspect

The slope's aspect influences the micro-climatic conditions and vegetation cover along the slope. Moreover, the slope aspect affects the weathering of bedrock and controls the pedogenesis [41].

The aspect map was obtained by processing the DEM of the area and sub-dividing it into 4 spatial classes (North, South, East, and West).

2.5.5. Distance from Watercourses

Streambank erosion processes can be important conditioning agents for instability. Moreover, it is supposed that the distance from the impluvia may be another key factor to characterize potential instability. The 'distance from the impluvia (watercourses)' map was derived from the hydrographic network map in vector format, which was produced by the Regione Piemonte (1:10,000 scale), and processed through the ArcGIS®software's (ESRI, Redlands, California, USA) 'path distance' function.

The map was sub-divided into 4 classes, grouping the areas as a function of distance from the impluvia and stream incisions. The fixed class thresholds were (1) 50 m, (2) 50–150 m, (3) 150–300 m, and (4) above 300 m.

The class of maximum landslide density included the buffer area between 50 and 150 m from the watercourses. The Landslide Susceptibility Index (LSI) was computed by considering the frequency of the various classes inside the study area, and the highest LSI was assigned to the areas located at a distance from watercourses farther than 300 m. This class, rather small with respect to the whole area under study (7.5% of the entire area), appears to be particularly extended in the surroundings of the Rovella mountain, which were severely hit by the instability processes that occurred during the 1968 event.

2.5.6. Land Use

Land use is an important factor in the definition of landslide susceptibility, because it influences the relationship between the permeable and impermeable surfaces exposed over the slopes. Moreover, it affects the rainwater flow behavior and the soil saturation. Land use data were obtained from the available aerial photographs relative to 1968. Photo-interpreted data were transposed on basic cartography and validated through land surveys in detail. Then, data were digitized in order to draw a land use map in raster format.

The map classified the areas according to 6 different uses: (1) wood, (2) thin wood, (3) grassland/pastureland, (4) urban fabric, (5) sparse urbanization, and (6) industrial plants. Data showed that the majority (82%) of landslides that occurred during the 1968 event affected wood-covered slopes (Figure 6). However, the current state of knowledge did not allow inference of the impact the wood cover had on the slope stability. Thus, the land use factor was not included in the LSI map elaboration.
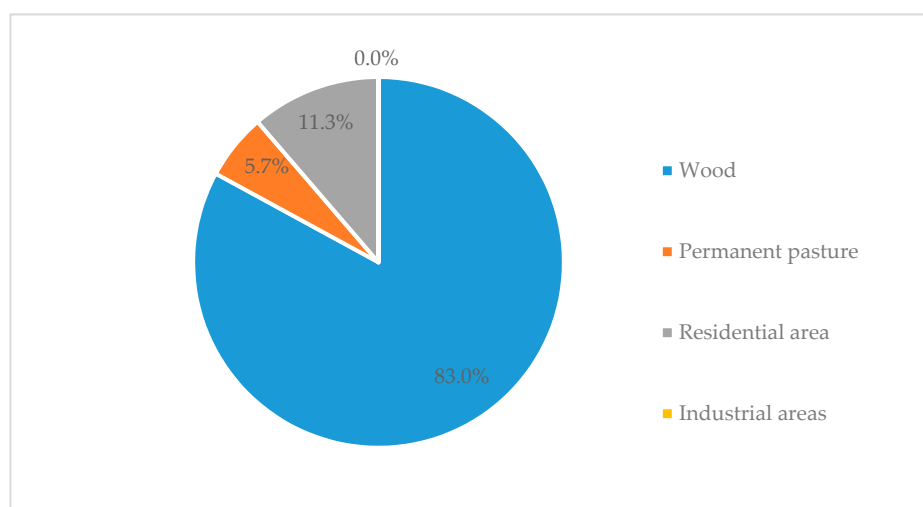
**Figure 6.** Landslide distribution in relation to land use.

3. Results

3.1. Lithology

First, the relationship between stability and the lithological classes (Figure 4) was considered, in order to determine the relevance of each layer class with respect to its areal extension. In particular, this relationship is expressed through the Landslide Susceptibility Index relative to each of the j-th factors being considered (LSI$_{rel,j}$) [19]. Then, the obtained values were re-classified according to a scale from 1 to 100 (100 maximum value) to define the susceptibility in relation to each class for the considered case study (Table 3). Then, the data were synthesized in the corresponding thematic map (Figure 7).

Table 3. Re-classified lithology impact factor.

Lithology	IF$_{rel}$
Biotitic gneiss	76
Leucogranites	39
Gabbros	82
Ultrafemic rocks	0
Alluvial deposits	12
Gravel deposits	33
Gravitative deposits	34
Kinzigite rocks	100
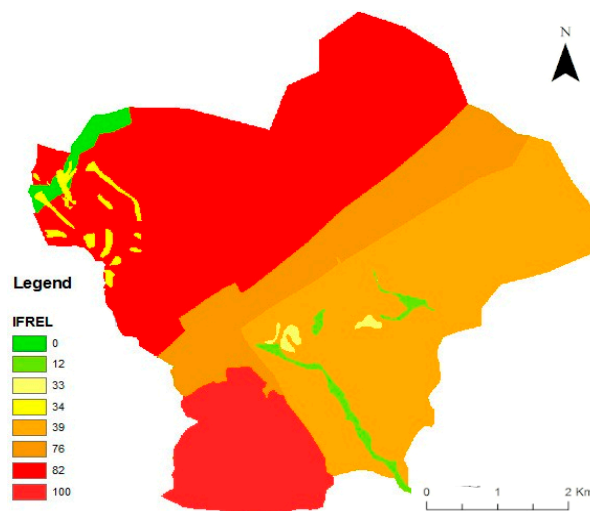
Figure 7. Relative Landslide Susceptibility Index (IF$_{rel,j}$) for each lithology class.

3.2. Morphology

Slope morphology, according to three categories (convex, concave, and plane), was based on the areal ratio between the observed unstable and stable surfaces (Table 4). The relative landslide indexes were identified and mapped (Figure 8).

Table 4. Re-classified morphology impact factor.

Morphology of Slopes	IF$_{rel}$
Concave	100
Plane	89
Convex	75
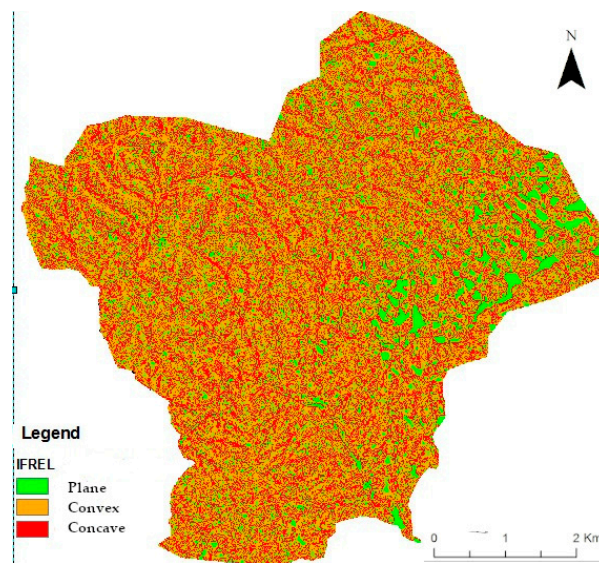
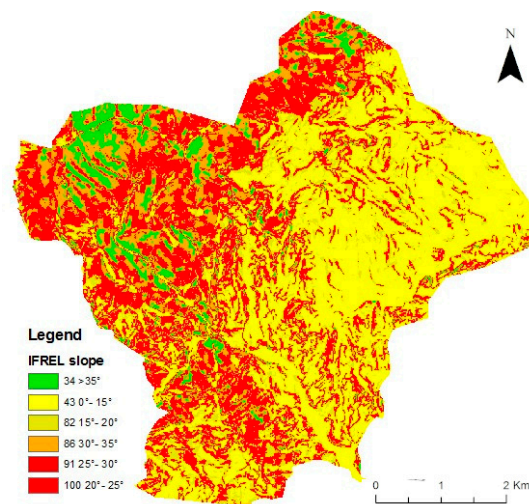**Figure 8.** Relative Landslide Susceptibility Index (LSI$_{rel,j}$) for each morphology class.

3.3. Slope

The majority (83%) of recorded landslides occurred within the slope class of 15–35°. This fact is in agreement with what was previously known in the literature [42,43]. Among the 4 slope classes, the distribution of landslides was almost uniform. The frequency of instability processes sharply diminished for slopes lower than a 15° dip (10% of the processes recognized). This depends on the general equilibrium conditions, which characterize low-angle slopes. Similarly, a marked reduction of the landslide occurrence (8%) emerged for slope angles above 35° (Figure 9). As confirmed by on-site observations, this might be caused by the reduction of soil thickness, which is a function of slope-dip growth. In particular, colluvial cover decreases until the bare rock becomes exposed. Coherently, the amount of movable materials during heavy, erosive rainfall events declines until it is minimized.
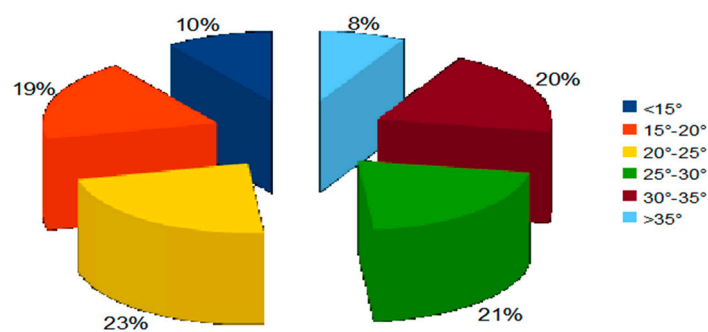
Figure 9. Instability processes occurrence (%) as a function of dip-slope classes, reported as different dip-slope ranges, represented with different colors.

Based on the relationship between landslide and stable areas with respect to the fixed slope-dip classes, the relative 'Landslide Indexes' were computed. The inferred values showed that the majority of the landslide-prone areas (almost 50% of the identified processes) occurred in the dip interval between 20 and 30° (Figure 10).
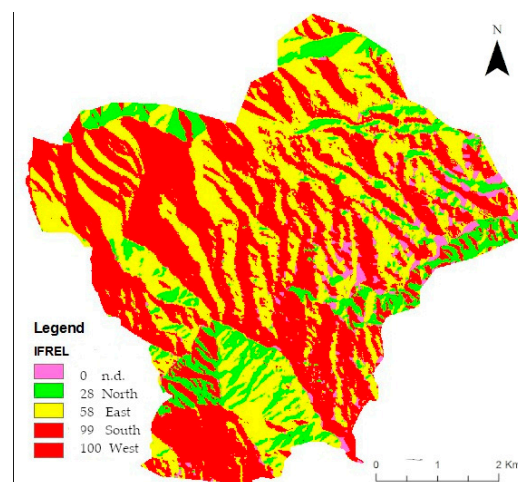
Figure 10. Map of the Relative Landslide Susceptibility Index (LSI$_{rel,j}$) in front of the 'dip-slope' factor.

3.4. Aspect

An aspect value was assigned corresponding to the number of landslides detected in relation to its detected detachment niche. Data showed that the north-facing slopes were scarcely affected (5% of the cataloged processes) by landslides. Conversely, south-facing slopes contained the highest incidence of gravitational processes (48%).

North-facing slopes only accounted for 14% of the total surface in the study area. Instead, south- and east-facing slopes were predominant. Considering the relationship between 'landslide' and 'no landslide' pixels, the greatest susceptibility was observed in relation to the west- and south-facing classes (Figure 11).
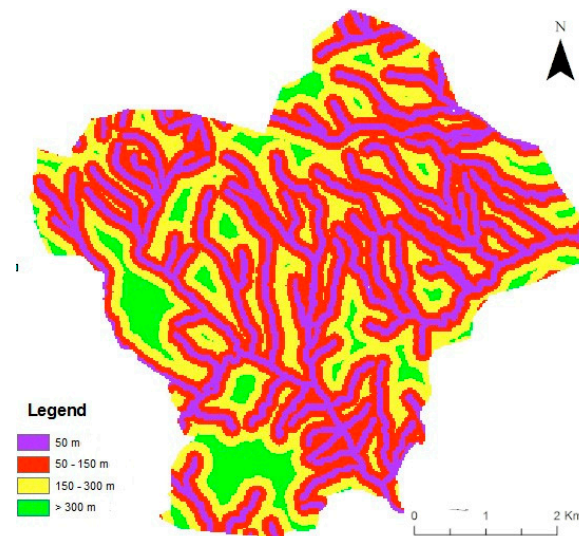

Figure 11. Relative Landslide Susceptibility Index (LSI$_{rel,j}$) as a function of the aspect factor (n.d. is used in the map for the areas where the aspect is not definable, due to the poor level of detail of the available raster)

3.5. Distance from Watercourses

The estimated LSI values in relation to the distance from watercourses, as mapped in Figure 12, appeared to be contradictory both with respect to the expected results and the experimental evidence. It was hypothesized that the most prone class could be the one closest to watercourses (i.e., distance shorter than 50 m). The discrepancy between the expected and the real results could depend upon the stream network map scale and the scarce level of detail in the available cartography, where low-order

stream segments were omitted. This could explain the singular attribution of the Rovella mountain landslides to a high distance class. In fact, this sub-area, noteworthy because it is located far from the main watercourses, was affected by several low-order incisions.

Figure 12. Relative Landslide Susceptibility Index (LSI$_{rel,j}$) as a function of the distance from watercourses.
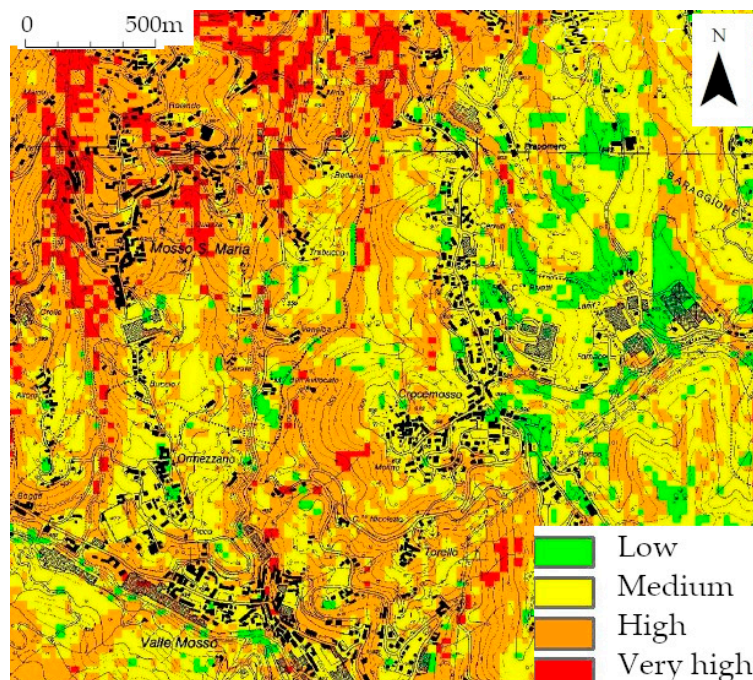
3.6. Final Landslide Susceptibility Map

First, the relevance of each chosen control factor for instability was determined, as reported in Figure 13. Lithology appeared to be the most relevant factor in controlling the slope stability (23%). As already shown, shallow landslides only involved the soil layer (0.5 m thick, with a maximum depth of between 2 and 3 m). The mother rock, only emerging in restricted land portions (narrow torrent incisions above 1300 m above sea level), was hardly affected. The relationship with the bedrock emerges through the eluvium-related soils' granulometry, which is related to different geo-mechanical characteristics. In particular, in the area under study, the gabbro predominates (40%), followed by biotite-bearing leucogranite (31%) and biotitic gneiss (14%).
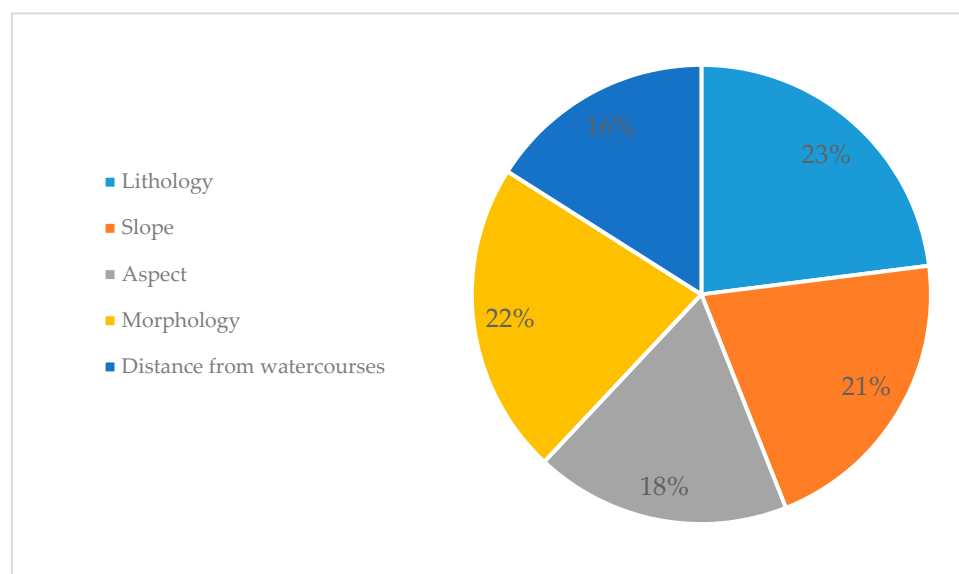
Figure 13. Percent weight of all the slope stability-inducing factors.

Slope inclination is another relevant factor [42,43]. Nearly 50% of the observed processes occurred for dipping angles between 20 and 30°. A lower landslide susceptibility was calculated for the sectors with slope angles between 0 and 20° and those above 35°. On-site surveys confirmed these results, depending on the decline of the eluvial and colluvial cover depth, above a given slope steepness and up to the bare soil outcrop.

Finally, a susceptibility map in raster format was produced, representing the landslide susceptibility for the area under study. The data were classified according to different susceptibility classes (Low, Middle, High, and Very High). This classification was obtained through the natural breaks (algorithm of Jenks) classification method [44]. An extract of the susceptibility map is shown in Figure 14.


Figure 14. Extract of the susceptibility map obtained for the area under study.

3.7. Results Validation

In order to test the predictive ability of the susceptibility map, a verification dataset of observed landslides was used as a parallel input. The data, derived from direct field observations, belong to two different events that occurred in the same area in October 2000 and November 1994. The cartographic bases for the identification of landslides (scale 1:5000) were the geo-morphological map and the geo-hydrological instability processes map of the municipality of Valle Mosso, belonging to the same area mapped in the susceptibility map. The landslide positions were digitized as a punctual shapefile called 'Landslide Validation'. Subsequently, in coincidence with each landslide, using the ArcGIS function 'Extract Values to Point', the local susceptibility values were extracted from the raster of the Total Landslide Susceptibility Index (in pixels). Thus, it was possible to find the susceptibility category in relation to each observed instability phenomenon. Figure 15 shows the obtained results of validation process.

In particular, 67% of landslides belonging to the test dataset (used for the validation) fell into the 'Very High' susceptibility class, 24% fell into the 'High' susceptibility class, while only 9% belonged to the 'Middle' or 'Low' classes.
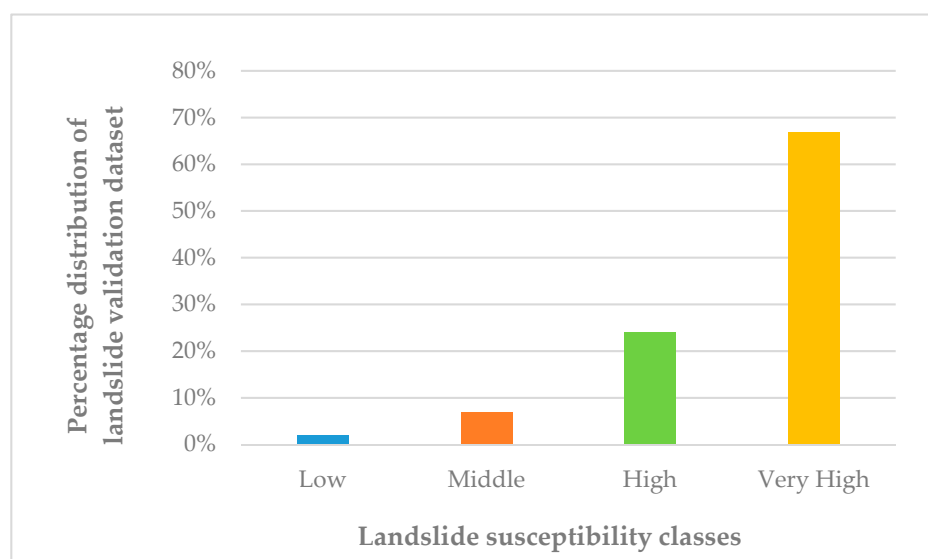
Figure 15. Results of validation process, using 1994 and 2000 landslides as the validation dataset. The majority of observed landslides fell within the 'Very High' (67%) or 'High' (24%) susceptibility classes.

4. Discussion

The final landslide susceptibility map, based on factors with similar characteristic timescale dynamics, allowed the evaluation of the potential slope instability of the area under study through different sensitivity factors. These analyses were originally used for the management of landslide hazards and risks [45,46]. In particular, qualitative and quantitative approaches were developed to realize inventory maps, relating to landslide predisposing and triggering factors [28]. This was especially possible thanks to the use of GIS platforms [47–50]. In order to apply a sensitivity assessment, the literature proposed different methods, including probabilistic approaches [51], statistical analyses [52–57], physical methods [58,59], or machine learning [60–62].

Implementing the original susceptibility calculation method, past extreme geo-hydrological events and susceptibility factors were combined in the vulnerability estimation of the area under study. In particular, through the integration of historical and geo-morphological data, a database with 148 flood/landslide events that affected the area under study was created. Then, a classification of factors was implemented, based on the technical map of the region of interest (scale: 1:10,000). Owing to the potentialities offered by the use of GIS platforms, these maps can be used and shared for land planning and civil protection activities.

Applying this approach, it was possible to assess the geographical distribution of the events and the relevance of each triggering factor, also known as a predisposing factor, which refers to the slope's internal conditions [63]. The results confirm the relevance of these factors, as shown by a recent literature review on this topic [64]. Lithology appeared to be the most relevant landslide susceptibility factor. The literature confirms that, as observed in the case study, volcaniclastic rocks, containing highly weatherable minerals, are more prone to the development of shallow instability phenomena than intrusive rocks [65]. Morphology, slope, and aspect were the other relevant factors, in order of magnitude identified by this study. In this respect, considering that the data were extracted from DEM map elaborations, a previous study showed that 10-m spatial resolution DEMs, jointly with the identification of landslide source areas, represent the best possible choice for the preparation of susceptibility maps [66].

Several works included the distance from watercourses as a key parameter in the evaluation of susceptibility [64]. None of them reported the contradictory results that we obtained. This confirms the need to improve the amount and quality of data with respect to this parameter in our case study. With respect to the relevance of watercourses, their artificialization should be mentioned. In fact,

as shown in several works, stemming from a historical analysis of relevant flooding and landslide events in different areas, the engineered transformation of river courses enables the significant alteration of the occurrence of instability phenomena [67–71].

In this case study, the poor quality of land use data, which referred to the period prior to the analyzed event, did not allow the inclusion of this parameter in the susceptibility final estimation. Previous studies have shown that land use, slope, and distance-to-river are less significant shallow landslide triggers [72]. The lower relevance of slope as a shallow landslide trigger cannot be confirmed by this study, since it ranked third. Considering the influence of the artificialization of rivers on landslide occurrence, the results with respect to this parameter might be contrasting. Finally, with respect to previous research, the relevance of land use and land use change as a relevant susceptibility factor was proved [73,74].

Following the approach used in this study might be a good option, thus excluding the factors characterized by short timescale dynamics. In fact, these parameters are strongly influenced by anthropogenic alterations of landscape, such as land use and distance-to-river, which might be altered by engineered works and new infrastructures. Moreover, this agrees with the approach that separates predisposing (internal) factors from external factors, such as rainfall [63]. This work excluded a discussion on the climate change impact on weather patterns, such as precipitation intensity, since it cannot represent a factor of intrinsic landscape vulnerability.

The method for landslide susceptibility mapping could be applied as one of the metrics of intrinsic environmental vulnerability of mountain areas in environmental impact assessment. In particular, the development of an integrated mapping tool can complement other methods already available from the literature and be applied to the sustainable development of projects and planning, due to its ability in evidencing the vulnerability of a territory with a sufficiently high spatial resolution and accuracy [75,76]. A further integration with other online tools could also serve as a basis for information sharing along the process of policy implementation by applying a bottom-up approach, as already suggested by the literature [77]. In fact, such representations can condense the meaningful indicators, converting them into augmented information, enabling them to become effective planning instruments [78–80].

5. Conclusions

The applied integrated method allowed the implementation of a zonation technique to assess the intrinsic environmental vulnerability of a test area with respect to landslide susceptibility. Such an approach allowed the determination of areas that were more prone to instability processes. By integrating different databases in a GIS environment and detailing the different factors that trigger the observed instability phenomena, it was possible to obtain an integrated digital representation, with the potential of it being continuously updated. The results, validated through an independent set referring to the same area under study, allowed the identification of different susceptibility classes. A very high percentage of observed slope processes fell under the categories of 'High' (24%) and 'Very High' (70%) susceptibility, showing the efficiency of the method. The validity of prior limiting the analyzed factors to the ones with similar dynamics timescales was also implicitly confirmed.

This GIS-based method can serve as a useful basis for planning and environmental impact assessment, thanks to the possibility of sharing the results among different users and stakeholders. Integrated and homogenized with other intrinsic vulnerability factors, it could also better support the implementation of local and regional informed policies for the sustainable development of vulnerable territories, such as mountains, and for infrastructures and projects to be developed in these areas.

Conflicts of Interest: The authors declare no conflict of interest.

References

1. Gardner, J.S.; Dekens, J. Mountain hazards and the resilience of social–ecological systems: Lessons learned in India and Canada. *Nat. Hazards* **2007**, *41*, 317–336. [CrossRef]

2. Flentje, P.N.; Chowdhury, R.N. Resilience and sustainability in the management of landslides. *Eng. Sustain.* **2018**, *171*, 3–4. [CrossRef]

3. European Union (EU). Directive 2014/52/EU of the European Parliament and of the Council of 16 April 2014 Amending Directive 2011/92/EU on the Assessment of the Effects of Certain Public and Private Projects on the Environment. Available online: eur-lex.europa.eu/legal-content/EN/TXT/?uri=celex%3A32014L0052 (accessed on 28 October 2019).

4. Del Campo, A.G. Mapping environmental sensitivity: A systematic online approach to support environmental assessment and planning. *Environ. Impact Assess. Rev.* **2017**, *66*, 86–98. [CrossRef]

5. Herath, S.; Wang, Y. Case Studies and National Experiences. In *Landslides—Disaster Risk Reduction*; Springer Verlag: Berlin/Heidelberg, Germany, 2009; pp. 475–497.

6. Kjekstad, O.; Highland, L. Economic and social impacts of landslides. In *Landslides—Disaster Risk Reduction*; Springer Verlag: Berlin/Heidelberg, Germany, 2009; pp. 573–587.

7. Highland, L.M.; Godt, J.W.; Howell, D.G.; Savage, W.Z. *El Nino 1997–98, Damaging Landslides in the San Francisco Bay Area*; U.S. Geological Survey Fact Sheet; U.S. Geological Survey: Reston, VA, USA, 1998; pp. 89–98.

8. Highland, L.M. *Landslide Types and Processes: U.S. Geological Survey Fact Sheet*; U.S. Geological Survey: Reston, VA, USA, 2004; pp. 2004–3072.

9. Li, T.; Wang, S. *Landslide Hazards and their Mitigation in China*; China Science Press: Beijing, China, 1992.

10. Mandle, L.; Bryant, B.P.; Ruckelshaus, M.; Geneletti, D.; Kiesecker, J.M.; Pfaff, A. Entry points for considering ecosystem services within infrastructure planning: How to integrate conservation with development in order to aid them both. *Conserv. Lett.* **2016**, *9*, 221–227. [CrossRef]

11. Alimohammadlou, Y.; Najafi, A.; Yalcin, A. Landslide process and impacts: a proposed classification method. *Catena* **2013**, *104*, 219–232. [CrossRef]

12. Camici, S.; Brocca, L.; Melone, F.; Moramarco, T. Impact of climate change on flood frequency using different climate models and downscaling approaches. *J. Hydrol. Eng.* **2014**, *19*, 04014002. [CrossRef]

13. Willeit, M.; Ganopolski, A.; Dalmonech, D.; Foley, A.M.; Feulner, G. Time-scale and state dependence of the carbon-cycle feedback to climate. *Clim. Dyn.* **2014**, *42*, 1699–1713. [CrossRef]

14. Scafetta, N. Discussion on the spectral coherence between planetary, solar and climate oscillations: a reply to some critiques. *Astrophys. Space Sci.* **2014**, *354*, 275–299. [CrossRef]

15. Casazza, M.; Alessio, S. Modeling theoretical radiative-dynamic response of tropospheric clouds to cosmic ray changes associated with Forbush Decrease events. *Adv. Space Res.* **2015**, *55*, 2678–2682. [CrossRef]

16. Scafetta, N. High resolution coherence analysis between planetary and climate oscillations. *Adv. Space Res.* **2016**, *57*, 2121–2135. [CrossRef]

17. Targulian, V.O.; Krasilnikov, P.V. Soil system and pedogenic processes: Self-organization, time scales, and environmental significance. *Catena* **2007**, *71*, 373–381. [CrossRef]

18. Morris, P.; Therivel, R. *Methods of Environmental Impact Assessment*, 3rd ed.; Routledge: London, UK; New York, NY, USA, 2009.

19. Lee, S.; Min, K. Statistical analysis of landslide susceptibility at Yongin, Korea. *Environ. Geol.* **2001**, *40*, 1095–1113. [CrossRef]

20. Roodposhti, M.S.; Aryal, J.; Pradhan, B. A Novel Rule-Based Approach in Mapping Landslide Susceptibility. *Sensors* **2019**, *19*, 2274. [CrossRef] [PubMed]

21. Sabokbar, H.F.; Roodposhti, M.S.; Tazik, E. Landslide susceptibility mapping using geographically-weighted principal component analysis. *Geomorphology* **2014**, *226*, 15–24. [CrossRef]

22. Harrison, J.F.; Chang, C.H. Sustainable Management of a Mountain Community Vulnerable to Geohazards: A Case Study of Maolin District, Taiwan. *Sustainability* **2019**, *11*, 4107. [CrossRef]

23. Guzzetti, F.; Carrara, A.; Cardinali, M.; Reichenbach, P. Landslide hazard evaluation: a review of current techniques and their application in a multi-scale study, Central Italy. *Geomorphology* **1999**, *31*, 181–216. [CrossRef]

24. Roccati, A.; Faccini, F.; Luino, F.; Ciampalini, A.; Turconi, L. Heavy Rainfall Triggering Shallow Landslides: A Susceptibility Assessment by a GIS-Approach in a Ligurian Apennine Catchment (Italy). *Water* **2019**, *11*, 605. [CrossRef]

25. Marrazzi, S. *Orographic Atlas of Alps (In Italian: Altante Orografico delle Alpi)*; Priuli & Verlucca: Pavone Canavese, Italy, 2005.

26. Tropeano, D.; Turconi, L. Using historical documents for landslide, debris flow and stream flood prevention. Applications in Northern Italy. *Nat. Hazards* **2004**, *31*, 663–679. [CrossRef]

27. Tropeano, D.; Turconi, L. Geomorphic classification of alpine catchments for debris-flow hazard reduction. In Proceedings of the Third International Conference on Debris-Flow Hazards Mitigation: Mechanics, Prediction and Assessment, Davos, Switzerland, 10–12 September 2003; pp. 1221–1232.

28. Palladino, M.R.; Viero, A.; Turconi, L.; Brunetti, M.T.; Peruccacci, S.; Melillo, M.; Luino, F.; Deganutti, A.M.; Guzzetti, F. Rainfall thresholds for the activation of shallow landslides in the Italian Alps: The role of environmental conditioning factors. *Geomorphology* **2018**, *303*, 53–67. [CrossRef]

29. Romeo, R.W.; Mari, M.; Floris, M.; Pappafico, G.; Gori, U. An Approach to Join the Spatial and Temporal Components of Landslide Susceptibility: An Application to The Marche Region (Central Italy). *Italy J. Eng. Geol. Environ.* **2011**, *2*, 63–78.

30. Lee, S.; Hong, S.M.; Jung, H.S. A support vector machine for landslide susceptibility mapping in Gangwon Province, Korea. *Sustainability* **2017**, *9*, 48. [CrossRef]

31. Govi, M.; Sorzana, P.F. Landslide susceptibility as a function of critical rainfall amount in Piedmont basin (Northwestern Italy). *Studia Geomorphol. Carpatho-Balc.* **1980**, *14*, 43–61.

32. Luino, F. Sequence of instability processes triggered by heavy rainfall in the Northern Italy. *Geomorphology* **2005**, *66*, 13–39. [CrossRef]

33. Roccati, A.; Luino, F.; Turconi, L.; Piana, P.; Watkins, C.; Faccini, F. Historical geomorphological research of a ligurian coastal floodplain (Italy) and its value for management of flood risk and environmental sustainability. *Sustainability* **2018**, *10*, 3727. [CrossRef]

34. Luino, F.; Nigrelli, G.; Turconi, L.; Faccini, F.; Agnese, C.; Casillo, F. A proper land-use planning through the use of historical research. *Disaster Adv.* **2016**, *9*, 8–19.

35. Italconsult. *Studi Preliminari Agli Interventi Di Ricostruzione e Sistemazione Delle Zone Alluvionate In Provincia Di Vercelli*; Ministero dei Lavori Pubblici: Provveditorato Regionale alle Opere pubbliche per il Piemonte: Torino, Italy, 1969.

36. Carraro, F.; Dal Piaz, G.V.; Govi, M.; Sacchi, R. *Il Dissesto Idrogeologico Del 2 Novembre 1968 Nel Bacino Della Strona a Monte Di Cossato*; Comitato Regionale per la Programmazione Economica del Piemonte: Torino, Italy, 1970; pp. 143–175.

37. Varnes, D.J. *Landslide Hazard Zonation a Review of Principles and Practice*; UNESCO: Paris, France, 1984.

38. Fell, R.; Corominas, J.; Bonnard, C.; Cascini, L.; Leroi, E.; Savage, W.Z.; On behalf of the JTC-1 Joint Technical Committee on Landslides and Engineered Slopes. Guidelines for landslide susceptibility, hazard and risk zoning for land-use planning. *Eng. Geol.* **2008**, *102*, 85–98. [CrossRef]

39. Pierson, T.C. Piezometric response to rainstorms in forested hillslope drainage depressions. *J. Hydrol. N. Z.* **1980**, *19*, 1–10.

40. Stanchi, S.; Freppaz, M.; Zanini, E. The influence of Alpine soil properties on shallow movement hazards, investigated through factor analysis. *Nat. Hazards Earth Syst. Sci.* **2012**, *12*. [CrossRef]

41. D'Agostino, V.; Marchi, L. Debris flow magnitude in the Alps: Data collection and analysis. *Phys. Chem. Earth Part C* **2001**, *26*, 657–663.

42. Crosta, G.B.; Dal Negro, P.; Frattini, P. Soil slips and debris flows on terraced slopes. *Nat. Hazards Earth Syst. Sci.* **2003**, *3*, 31–42. [CrossRef]

43. Jenks, G.F. *Optimal Data Classification for Choropleth Maps, Occasional Paper No. 2*; Department of Geography, University of Kansas: Lawrence, MA, USA, 1977.

44. Aleotti, P.; Chowdhury, R. Landslide hazard assessment: Summary review and new perspectives. *Bull. Eng. Geol. Environ.* **1999**, *58*, 21–44. [CrossRef]

45. Carrara, A.; Guzzetti, F. Techniques and Tools for Mapping Natural Hazards and Risk Impact on the Developed Environment. *Nat. Haz.* **1999**, *20*, 93–324. [CrossRef]

46. Van Westen, C.J.; Castellanos, E.; Kuriakose, S.L. Spatial data for landslide susceptibility, hazard, and vulnerability assessment: An overview. *Eng. Geol.* **2008**, *102*, 112–131. [CrossRef]

47. Carrara, A.; Cardinali, M.; Detti, R.; Guzzetti, F.; Pasqui, V.; Reichenbach, P. GIS techniques and statistical models in evaluating landslide hazard. *Earth Surf. Process. Landf.* **1991**, *16*, 427–445. [CrossRef]

48. Dai, F.C.; Lee, C.F. Landslide characteristics and slope instability modeling using GIS, Lantau Island, Honk Kong. *Geomorphology* **2002**, *42*, 213–228. [CrossRef]

49. Huabin, W.; Gangjun, L.; Gonghui, W. GIS-based landslides hazard assessment: An overview. *Prog. Phys. Geogr.* **2005**, *29*, 548–567. [CrossRef]

50. Cachon, J.; Irigaray, C.; Fernandez, T.; El Hamdouni, R. Engineering geology maps: Landslides and geographical information systems. *Bull. Eng. Geol. Environ.* **2006**, *65*, 341–411.

51. Catani, F.; Lagomarsino, D.; Segoni, S.; Tofani, V. Landslide susceptibility estimation by random forests technique: Sensitivity and scaling issue. *Nat. Hazard Earth Syst. Sci.* **2013**, *13*, 2815–2831. [CrossRef]

52. Baeza, C.; Corominas, J. Assessment of shallow landslide susceptibility by means of multivariate techniques. *Earth Surf. Process. Landf.* **2001**, *26*, 1251–1263. [CrossRef]

53. Youssef, A.M.; Pourghasemi, H.R.; Pourtaghi, Z.S.; Al-Katheeri, M.M. Landslide susceptibility mapping using random forest, boosted regression tree, classification and regression tree, and general linear models and comparison of their performance at Wadi Tayyah Basin, Asir Region, Saudi Arabia. *Landslides* **2016**, *13*, 839–856. [CrossRef]

54. Wang, P.; Bai, X.; Wu, X.; Yu, H.; Hao, Y.; Hu, B.X. GIS-based random forest weight for rainfall-induced landslide susceptibility assessment at a humid region in Southern China. *Water* **2018**, *10*, 1019. [CrossRef]

55. Goetz, J.N.; Brenning, A.; Petschko, H.; Leopold, P. Evaluating machine learning and statistical prediction techniques for landslide susceptibility modelling. *Comput. Geosci.* **2015**, *81*, 1–11. [CrossRef]

56. Guzzetti, F.; Stark, C.P.; Salvati, P. Evaluation of flood and landslide risk to the population of Italy. *Environ. Manag.* **2005**, *36*, 15–36. [CrossRef] [PubMed]

57. Zêzere, J.L.; Pereira, S.; Melo, R.; Oliveira, S.C.; Garcia, R.A.C. Mapping landslides susceptibility using data-driven methods. *Sci. Total Environ.* **2017**, *589*, 250–267. [CrossRef] [PubMed]

58. Long, N.T.; De Smedt, F. Analysis and mapping of rainfall-induced landslide susceptibility in a Luoi District, Thua Thien Hue Province, Vietnam. *Water* **2018**, *11*, 51. [CrossRef]

59. Chen, Z.; Wang, J. Landslide hazard mapping using logistic regression model in Mackenzie Valley, Canada. *Nat. Hazards* **2007**, *42*, 75–89. [CrossRef]

60. Pradhan, B.; Lee, S.; Buchroithner, M.F. A GIS-based back-propagation neural network model and its cross-application and validation for landslide susceptibility analysis. *Comput. Environ. Urban Syst.* **2010**, *34*, 216–235. [CrossRef]

61. Pham, B.T.; Pradhan, B.; Bui, D.T.; Prakash, I.; Dholakia, M.B. A comparative study of different machine learning methods for landslide susceptibility assessment: A case study of Uttarakhand area (India). *Environ. Model. Softw.* **2016**, *84*, 240–250. [CrossRef]

62. Valencia Ortiz, J.A.; Martínez-Graña, A.M. A neural network model applied to landslide susceptibility analysis (Capitanejo, Colombia). *Geomat. Nat. Hazards Risk* **2018**, *9*, 1106–1128. [CrossRef]

63. Pradhan, B. A comparative study on the predictive ability of the decision tree, support vector machine and neuro-fuzzy models in landslide susceptibility mapping using GIS. *Comput. Geosci.* **2013**, *51*, 350–365. [CrossRef]

64. Pourghasemi, H.R.; Yansari, Z.T.; Panagos, P.; Pradhan, B. Analysis and evaluation of landslide susceptibility: A review on articles published during 2005–2016 (periods of 2005–2012 and 2013–2016). *Arab. J. Geosci.* **2018**, *11*, 193. [CrossRef]

65. Sterling, S.; Slaymaker, O. Lithologic control of debris torrent occurrence. *Geomorphology* **2007**, *86*, 307–319. [CrossRef]

66. Schlögel, R.; Marchesini, I.; Alvioli, M.; Reichenbach, P.; Rossi, M.; Malet, J.P. Optimizing landslide susceptibility zonation: Effects of DEM spatial resolution and slope unit delineation on logistic regression models. *Geomorphology* **2018**, *301*, 10–20. [CrossRef]

67. Faccini, F.; Luino, F.; Paliaga, G.; Sacchini, A.; Turconi, L. Yet another disaster flood of the Bisagno stream in Genoa (Liguria, Italy): October the 9th–10th 2014 event. *Rend. Online Soc. Geol. Italy* **2015**, *35*, 128–131. [CrossRef]

68. Maraga, F.; Turconi, L.; Pellegrini, L.; Anselmo, V. Scouring in the Po river basin at the upper plain (Italy). In Proceedings of the Engineering Geology for Society and Territory, IAEG XII Congress, Torino, Italy, 15–19 September 2014; Springer: Cham, Switzerland, 2015; Volume 3, pp. 489–493.

69. Faccini, F.; Luino, F.; Paliaga, G.; Sacchini, A.; Turconi, L.; de Jong, C. Role of rainfall intensity and urban sprawl in the 2014 flash flood in Genoa City, Bisagno catchment (Liguria, Italy). *Appl. Geogr.* **2018**, *98*, 224–241. [CrossRef]

70. Paliaga, G.; Faccini, F.; Luino, F.; Turconi, L. A spatial multicriteria prioritizing approach for geohydrological risk mitigation planning in small and densely urbanized Mediterranean basins. *Nat. Hazards Earth Syst. Sci.* **2018**, *19*, 53–69. [CrossRef]

71. Roccati, A.; Faccini, F.; Luino, F.; De Graff, J.V.; Turconi, L. Morphological changes and human impact in the Entella River floodplain (Northern Italy) from the 17th century. *Catena* **2019**, *182*, 104–122. [CrossRef]

72. Al-Najjar, H.A.H.; Kalantar, B.; Pradhan, B.; Saeidi, V. Conditioning factor determination for mapping and prediction of landslide susceptibility using machine learning algorithms. In Proceedings of the Earth Resources and Environmental Remote Sensing/GIS Applications X, SPIE Remote Sensing, Strasbourg, France, 9–12 September 2019; International Society for Optics and Photonics: Bellingham, WA, USA, 2019; Volume 11156, 111560K. [CrossRef]

73. Youssef, A.M.; Pradhan, B.; Sefry, S.A.; Abu Abdullah, M.M. Use of geological and geomorphological parameters in potential suitability assessment for urban planning development at Wadi Al-Asla basin, Jeddah, Kingdom of Saudi Arabia. *Arab. J. Geosci.* **2015**, *8*, 5617–5630. [CrossRef]

74. Bathrellos, G.D.; Skilodimou, H.D.; Chousianitis, K.; Youssef, A.M.; Pradhan, B. Suitability estimation for urban development using multi-hazard assessment map. *Sci. Total Environ.* **2017**, *575*, 119–134. [CrossRef]

75. Zhang, Y.; Lu, W.X.; Guo, J.Y.; Zhao, H.Q.; Yang, Q.C.; Chen, M. Geo-Environmental impact assessment and management information system for the mining area, northeast China. *Environ. Earth Sci.* **2015**, *74*, 7173–7185. [CrossRef]

76. Chen, L.; Li, L.; Yang, X.; Zheng, J.; Chen, L.; Shen, Z.; Kervyn, M. A worst-case scenario based methodology to assess the environmental impact of land use planning. *Habitat Int.* **2017**, *67*, 148–163. [CrossRef]

77. Xue, J.; Liu, G.; Casazza, M.; Ulgiati, S. Development of an urban FEW nexus online analyzer to support urban circular economy strategy planning. *Energy* **2018**, *164*, 475–495. [CrossRef]

78. Janssen, M.; Wimmer, M.A. Introduction to Policy-Making in the Digital Age. In *Policy Practice and Digital Science*; Springer International Publishing: Cham, Switzerland, 2015; pp. 1–14.

79. Lega, M.; Casazza, M.; Teta, R.; Zappa, C.J. Environmental impact assessment: A multi-level, multi-parametric framework for coastal waters. *Int. J. Sustain. Dev. Plan.* **2018**, *13*, 1041–1049. [CrossRef]

80. Liu, G.; Yin, X.; Pengue, W.; Benetto, E.; Huisingh, D.; Schnitzer, H.; Wang, Y.; Casazza, M. Environmental accounting: In between raw data and information use for management practices. *J. Clean. Prod.* **2018**, *197*, 1056–1068. [CrossRef]